

Quantifying the irregularity of a time series

Max Potratzki,^{1,2} Manuel Adams,^{1,2} Timo Bröhl,^{1,2} and Klaus Lehnertz^{1,2,3}

¹*Department of Epileptology, University of Bonn Medical Centre, Venusberg Campus 1, 53127 Bonn, Germany*

²*Helmholtz Institute for Radiation and Nuclear Physics,
University of Bonn, Nussallee 14–16, 53115 Bonn, Germany*

³*Interdisciplinary Center for Complex Systems, University of Bonn, Brühler Straße 7, 53175 Bonn, Germany*

(*klaus.lehnertz@ukbonn.de)

(Dated: December 9, 2025)

We introduce circulance, a scalar measure for classifying time series of dynamical systems. Circulance captures the extent of temporal regularity or irregularity that is encoded in the topology of a directed ordinal pattern transition network derived from a time series. We demonstrate numerically that circulance sensitively and robustly positions time series of canonical model systems, representative of preset dynamical regimes, along a continuous spectrum from regularity to randomness. Analyzing empirical data from long-term observations of high-dimensional, complex systems – human brain and the Sun – reveals that circulance aids in elucidating different dynamical regimes.

I. INTRODUCTION

Investigations of dynamical systems often depend on time series data. A central task is to classify the behavior of a system and how it may evolve over time. Identifying regularity in a time series and its potential breakdown is crucial for understanding the underlying dynamics, distinguishing between periodic, quasiperiodic, chaotic, and stochastic behavior, and for assessing a system's stability. However, identifying regularity in practice is fraught with difficulties. Empirical time series may be contaminated with measurement noise and other unwanted external disturbances and may reflect transient dynamics. These challenges are compounded when deviations from regularity are subtle, gradual, or localized in time. Beyond classifying a system's dynamics as regular or not, it is therefore of high interest to position the dynamics along a spectrum ranging from strictly periodic via chaotic to fully stochastic.

Several methods for the classification of time series have been proposed and critically discussed [1–17]. Although powerful in many contexts, these methods typically focus on detecting the presence of dominant periodic components in either the time domain, frequency domain, the system's reconstructed phase space or by representing the time series as a network. Only a few methods provide a classification and only within parts of the continuum from strictly periodic to fully stochastic [18–34], yet not the full spectrum. Moreover only few methods are explicitly designed to handle data from non-stationary systems [35–41]. These limitations necessitate the development of a flexible and advanced approach to time series classification.

Here, we present a novel approach for a quantitative classification of a time series derived from a suitable observable of a complex dynamical system. It has been shown that probabilities of transitions between ordinal patterns derived from time series encapsulate vital information about a system's dynamics [42–46]. These transitions can be topologically represented as ordinal pattern

transition networks (OPTNs) [28, 46–48]. We leverage graph-theoretical metrics – fundamentally a vertex' in- and out-degree – to investigate the intricate topological properties of these networks constructed from time series data. Specifically, we assess to what extent an OPTN's topology deviates from a circular structure and quantify this extent with a single scalar measure, to which we refer as circulance in the following. We demonstrate that an OPTN's circulance encodes essential dynamical aspects of a time series, which allows a quantitative distinguishing of dynamical regimes across diverse synthetic and empirical datasets.

II. METHODS

A. From a Time Series to an OPTN

A time series $\xi(t)$, with $t \in \mathbb{N}_0^+$, $t \in [0, N - 1]$, is divided into partitions $p(s)$ (with running index $s \in \{0, 1, \dots, N - 1 - (d - 1)\tau\}$) of size d (embedding dimension), with each of the elements of $p(s)$ being separated by τ time steps (embedding delay). From each partition $p(s)|_{s=t'}$, an ordinal pattern $q(s)|_{s=t'}$ is inferred by a rank-ordering of the elements of the partition [42] $p(s)|_{s=\{t'\}} = [\xi(t'), \xi(t' + \tau), \dots, \xi(t' + (d - 1)\tau)]$, where $t' \in \{0, 1, \dots, N - 1 - (d - 1)\tau\}$. With $\mathcal{X}_{t'} = \{\xi(t'), \xi(t' + \tau), \dots, \xi(t' + (d - 1)\tau)\}$, the rank ordering function ρ^* can be defined as

$$\rho^* : \mathcal{X}_{t'} \rightarrow \mathbb{N}_0,$$

such that

$$\rho^*(u) = |\{v \in \mathcal{X}_{t'} | u < v\}|, \quad (1)$$

where $u, v \in \mathcal{X}_{t'}$. Therefore, $q(s)$ is a sequence of unique ordinal patterns. As $d!$ unique ordinal patterns are possible, the unique ordinal pattern \hat{q}_m ($m \in [0, d! - 1]$) is obtained by ordering the unity ordinal pattern $\hat{q}_1 = (0, 1, \dots, d - 1)$ according to the permutation $\rho(\mathcal{X}_{t'})$:

$$\rho : \mathcal{X}_{t'}^d \rightarrow \mathbb{N}_0^d,$$

with

$$\begin{aligned} \rho(\mathcal{X}_{t'}) &= (\rho^*(\xi(t')), \rho^*(\xi(t' + \tau)), \\ &\dots, \rho^*(\xi(t' + (d-1)\tau))), \end{aligned} \quad (2)$$

such that

$$\begin{aligned} \hat{q}_i &= (0, 1, \dots, d-1)_{\rho(\mathcal{X}_{t'})} \\ &= (0_{\rho^*(\xi(t'))}, 1_{\rho^*(\xi(t'+\tau))}, \dots, (d-1)_{\rho^*(\xi(t'+(d-1)\tau))}). \end{aligned} \quad (3)$$

To illustrate the derivation of a unique ordinal pattern, consider the partition $p(s) = (0.2, 0.9, -0.48, -0.78)$, whose elements form the set $\mathcal{X}_{t'} = \{0.2, 0.9, -0.48, -0.78\}$, for some s and some t' (cf. Fig. 1 (a)). Now as $\rho(\mathcal{X}) = (2, 3, 1, 0)$, this results in the corresponding unique ordinal pattern $\hat{q}_m = (0_2, 1_3, 2_1, 3_0) = (3, 2, 0, 1)$ for some m . By convention, in the case of repeated amplitude values ranks are assigned according to the order of temporal occurrence, e.g., $p(s) = (1, 1, 1, 1)$ leads to $\hat{q}_m = \hat{q}_1$. Therefore, constant amplitudes yield the same unique ordinal pattern as strictly increasing amplitudes.

An OPTN can be represented by a directed graph $\mathcal{O} = \{\mathcal{V}, \mathcal{E}\}$ consisting of a set of vertices \mathcal{V} (with $V = |\mathcal{V}|$ elements) and a set of directed edges \mathcal{E} (with $E = |\mathcal{E}|$ elements). Having transformed a time series to a sequence of ordinal patterns, we can now construct a topological representation of the transitions between successive patterns [48]. To do so, each unique ordinal pattern \hat{q}_i is associated with a vertex $v_i \in \mathcal{V}$ ($i \in [0, V-1]$) in the OPTN. An edge $e_{ij} \in \mathcal{E}$ exists between vertices v_i and v_j , if there is a transition from pattern \hat{q}_i to pattern \hat{q}_j in the temporal sequence of ordinal patterns $q(s)$. Therefore, vital topological aspects of the OPTN can be represented as an adjacency matrix \mathbf{A} with $A_{ij} = 1$ if e_{ij} exists, and $A_{ij} = 0$ otherwise. Self-loops – transitions from a pattern \hat{q}_i onto itself – are not considered ($A_{ii} = 0$), as they do not represent a change in the prevailing dynamics. The (ir)regularity of a time series is translated to a topological level of an OPTN, as shown in Figure 1.

B. Defining Circulance

1. Capturing distinct transitions between unique ordinal patterns

The in- and the out-degree $k_{v_i}^\mp$ of vertex v_i in an OPTN assess the amount of unique ordinal patterns directly preceding (in-degree) respectively following (out-degree) the unique ordinal pattern \hat{q}_i associated with v_i and are defined as

$$k_{v_i}^- = \sum_{v_j \in \mathcal{V}} A_{ji}, \quad k_{v_i}^+ = \sum_{v_j \in \mathcal{V}} A_{ij}. \quad (4)$$

Since an OPTN retains essential aspects of a time series [47] – provided embedding parameters d and τ were

chosen appropriately – we conjecture that the in- and out-degrees provide a means of characterizing this time series and potentially differentiating between dynamical regimes. Generally, each dynamics exhibited by the system over a given time interval exceeding $(d-1)\tau$ may be represented as a sequence of ordinal patterns and therefore as a walk on the OPTN. Strictly periodic dynamics translate to a chordless cycle (Fig. 1).

The possibility to pursue a closed trail in a directed network is largely reflected by the vertices' in- and out-degrees. We therefore consider the normalized in- and out-degree distributions $\Gamma^\mp(k^\mp)$ of the OPTN to exhibit specific properties depending on the system's dynamics. A strictly periodic time series satisfies the condition $\xi(t+T) = \xi(T)$ with period $T \in \mathbb{N}^+$, translating to a repeating temporal sequence of ordinal patterns. This resembles a walk in circles on the OPTN, as further reflected by the OPTN's circular structure with all vertices having the same in- and out-degrees $k = k^+ = k^-$ (excluding the case of a fully connected network). Consequently, the normalized degree distributions $\Gamma^\mp(k^\mp)$ take the form $\Gamma^\mp(k^\mp) = \delta_k(\mathcal{K}^\pm)$, where \mathcal{K}^\pm denote the sets of in-/out-degrees, with $k^\pm \in \mathcal{K}^\pm$ and $k \in \mathbb{N}^+$, and δ_k denotes the Dirac measure, such that

$$\sum_{v_i \in \mathcal{V}} k_{v_i}^- = \sum_{v_i \in \mathcal{V}} k_{v_i}^+ = |\mathcal{E}|. \quad (5)$$

Hence, for a strictly periodic time series – representing the left end of the spectrum of dynamical regimes – it then holds $|\mathcal{K}^+| = |\mathcal{K}^-| = 1$.

Deviations from strict periodicity lead to an increase in the number of different in- and out-degrees, depending on the specific dynamics (encoded as different colors in Fig. 1). We refer to the amount of degree values that are contained in \mathcal{K}^+ while also being in \mathcal{K}^- as (qoppa \wp):

$$\wp_\tau = |\mathcal{K}^+ \cap \mathcal{K}^-|. \quad (6)$$

This property has an indirect dependence on the embedding delay τ as the latter can determine topological aspects of the OPTN such as the in- and out-degrees of the vertices. We recall that we generally have to assume the time series sufficiently captured a suitable observable of the underlying system dynamics to allow any conclusion about the dynamical system itself. This is not universally given, particularly not for high-dimensional dynamical systems. A purely stochastic time series, such as that of a white noise process, represents the other extreme (right end) in the spectrum of dynamical regimes, and therefore poses a reasonable reference [49] to determine a sufficient embedding dimension for the construction of an OPTN.

2. Influence of time series length and embedding parameters

For a stochastic time series of length $N \sim N_q$, $N_q \rightarrow \infty$, an embedding dimension d would translate to an OPTN with each of the $V = d!$ possible unique ordinal patterns constituting a vertex. Consequently, it is

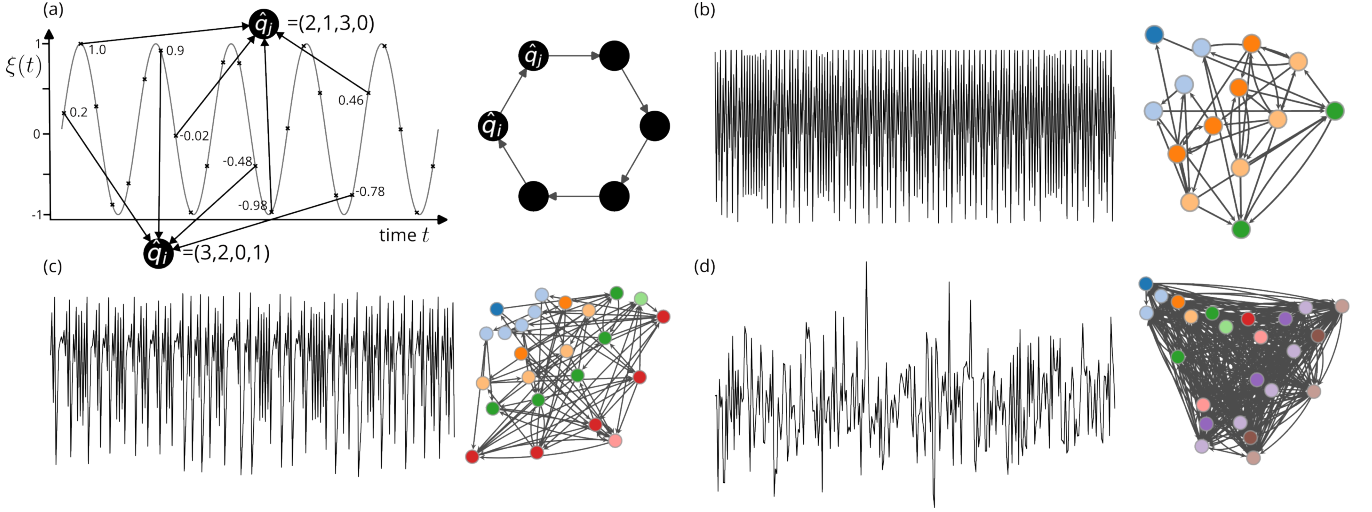


FIG. 1. Different types of dynamics and the corresponding ordinal pattern transition networks (OPTNs). Within each subfigure, vertices of the same color have the same number of adjacent vertices. (a) Schematic of the construction of an OPTN from a strictly periodic dynamics (with $d = 4$ and $\tau = 1$). The resulting OPTN consists of one closed trail or circuit on the OPTN. (b) A quasiperiodic dynamics results in a broader degree distribution (more distinct colors) of the OPTN. (c) Chaotic and (d) stochastic dynamics result in even more vertices and a higher amount of vertices with a distinct number of adjacent vertices in the respective OPTN. For a stochastic dynamics, the deviation from a simple circuit is maximum. Time series shown in (b)-(d) are of same length N .

to be expected that every possible transition between all pairs of unique ordinal patterns is observed in the temporal sequence of ordinal patterns, resulting in $E_{\max} = V(V - 1) = d!(d! - 1) \simeq d!^2$ edges in the OPTN.

Let us consider a case where $N_q \gg E_{\max}$. Consequently, the in- and out-degree distributions of the respective OPTN are rather homogeneous, as the OPTN is densely connected and approaches a fully connected network. Therefore, each vertex has approximately the same large degree. An opposing case would be constituted by $N_q \ll E_{\max}$. Here, the number of both unique ordinal patterns and unique transitions present in the temporal sequence of ordinal patterns does not even approximately amount to the number of all possible unique ordinal patterns and transitions. Only a very small subset of all possible transitions can be observed, and each of these transitions occurs randomly and rarely, resulting in a sparse OPTN with few low-degree vertices and a homogeneous degree distribution.

In between the two cases, we can further assume a scenario for which $N_q \sim E_{\max}$ holds. Only a fraction of possible unique ordinal patterns and transitions is observed. Different transitions are unevenly distributed, translating to a heterogeneous degree distribution of the respective OPTN. Consequently, and to guarantee maximum separability between a chaotic and a stochastic time series of length N we choose the embedding dimension d , such that

$$N \sim d!^2. \quad (7)$$

Due to the ambiguity of choosing an embedding de-

lay, we propose to calculate \mathfrak{Q}_τ for OPTNs constructed with embedding delays $\tau \in [2, \dots, \tau_{\max}]$, with τ_{\max} chosen such that at most 10% of the number of data points is lost (i.e., $(d - 1)\tau_{\max} = N/10$) when deriving the ordinal pattern sequence.

3. Circulance

For the final definition of circulance, we consider the time delay that minimizes \mathfrak{Q}_τ , since periodicity can not be artificially induced by an inappropriate choice of the embedding delay [1]. Eventually, with a sufficiently chosen embedding dimension d , we define circulance $\mathfrak{Q} \in \mathbb{N}^+$ as (Qoppa \mathfrak{Q}):

$$\mathfrak{Q} = \min \mathfrak{Q}_\tau. \quad (8)$$

The less regular (or periodic) a time series is the larger is the time series' circulance. The left end of the spectrum of dynamical regimes, that range from periodic over quasiperiodic and chaotic to stochastic, is located at $\mathfrak{Q} = 1$, independent of the length of the investigated time series, provided that at least one period has been captured. The right end of the spectrum does depend on the length of the investigated time series, and is determined by \mathfrak{Q} of a stochastic time series of the same length (cf. Eq. 7 and Fig. 2).

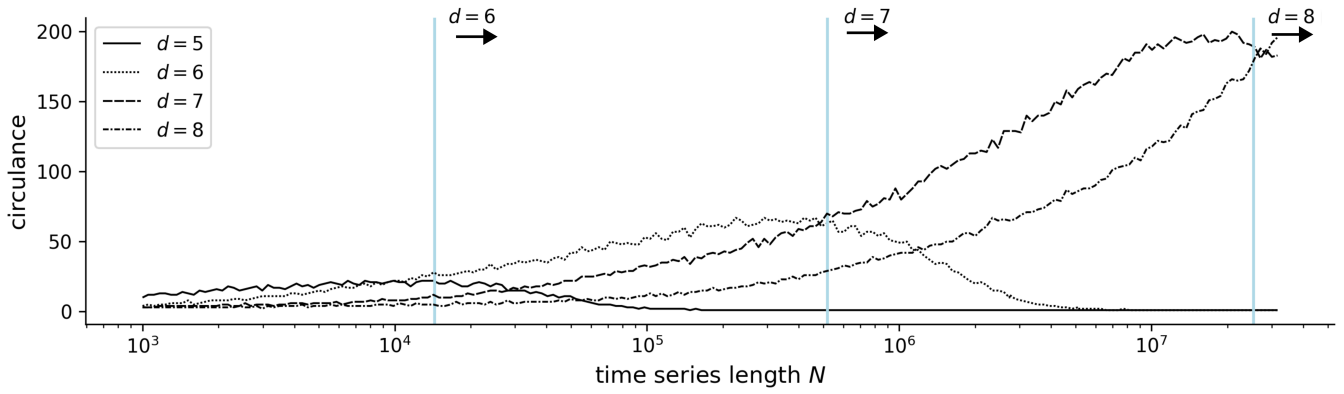


FIG. 2. Circulance \mathcal{Q} in dependence of time series length N for a single realization of a stochastic process and different embedding dimensions d . For a given time series length N , the embedding dimension d is chosen such that circulance is maximum. Blue vertical lines mark $N = d!^2$ (cf. Eq. 7).

III. INVESTIGATED SYSTEMS

A. Model Systems

We validate our approach using time series generated from various canonical dynamical systems (see Appendix A), capable of exhibiting distinct dynamical regimes in the continuum from strictly periodic over chaotic to stochastic, predetermined by the choice of the systems' control parameters. Embedding dimensions are chosen based on the lengths of the respective time series (see Figure 2). All continuous-time systems are integrated using a fourth-order Runge-Kutta method with adaptive step size control. Sampling rates are chosen to ensure adequate temporal resolution while avoiding oversampling artifacts. For discrete maps, iterations are performed directly. Time series have a length N after discarding transients.

B. Real World Systems

To assess the applicability of circulance to empirical data, we here analyze time series of two high-dimensional, complex systems – human brain and the Sun – for which long-lasting recordings of their dynamics are available. The exact nature of these dynamics is matter of ongoing debate, and previous research often renders the respective dynamics seemingly stochastic. We here investigate whether circulance can aid in elucidating the intricate characteristics of such complex dynamics.

1. Human Brain Dynamics

As a first example, we consider multichannel EEG data that was continuously recorded for three days from a healthy subject. The subject had signed informed consent that their clinical data might be used and published

for research purposes, and the study protocol had previously been approved by the local ethics committee. EEG electrodes were placed according to the International 10-20 system [50] with position Cz serving as physical reference. Data were sampled at 256 Hz using a 16 bit analog-to-digital converter and bandpass filtered offline between 1 - 45 Hz (4th order Butterworth characteristic). A notch filter (3rd order) was used to suppress contributions at the line frequency (50 Hz). We visually inspected the continuous recording for strong artifacts (e.g., subject movements or amplifier saturation) and excluded such data from further analyses.

2. Solar Magnetic Activity

As a second example, we consider multi-decade sunspot number records, associated with solar magnetic activity [51]. The recording of daily observations spans the years 1858 to 2018 and is provided by the World Data Center SILSO (Solar Influences Data Analysis Center) [52].

IV. RESULTS

A. Model Systems

We begin by demonstrating the merit of circulance by analyzing time series of length $N = 10000$ from a range of canonical dynamical systems and summarize our findings in Table I. The comparison against ground-truth and referencing against stochasticity allows a quantitative assessment of circulance's ability to correctly identify dynamical regimes. For strictly periodic time series, circulance consistently [53] attains its minimal value ($\mathcal{Q} = 1$), reflecting the uniform circular structure of the corresponding OPTNs. For stochastic time series, we observe highest circulance values ($\mathcal{Q} \geq 18$), approaching

dynamics/system	τ_{\min}	V	E	\mathfrak{Q}	observable
superimposed sine waves	2	18	18	1	
	2	18	18	1	
	2	18	18	1	
sawtooth	2	18	18	1	
v. d. Pol oscillator					<i>x</i> -component
periodic	7	30	30	1	
periodic	12	30	30	1	
FHN oscillator					<i>x</i> -component
quasiperiodic	6	38	75	3	
quasiperiodic	183	84	151	3	
coupled FHN osc.					mean <i>x</i> -comp.
quasiperiodic	17	30	43	2	
quasiperiodic	9	268	456	4	
chaotic	26	708	2787	8	
Hénon map					<i>x</i> -component
quasiperiodic	3	32	76	4	
chaotic	3	284	1142	7	
chaotic	53	720	8429	10	
Lorenz oscillator					<i>x</i> -component
quasiperiodic	13	66	80	2	
quasiperiodic	2	42	81	4	
stochastic	16	720	9793	18	

TABLE I. Circulance \mathfrak{Q} for different types of known dynamics of well-studied model systems for appropriately chosen control parameters (see Appendix A). Time series had a length $N = 10000$, which led us to choose an embedding dimension $d = 6$. τ_{\min} denotes the embedding delay that minimizes \mathfrak{Q}_τ , and V and E are the number of vertices and edges of the respective OPTN.

the upper bound of the spectrum ($\mathfrak{Q} = d!$), which depends on the network size (number of vertices) and the length of the time series N (see Eq. 7). In comparison to periodic time series, quasiperiodic time series yield slightly elevated circulance values ($2 \leq \mathfrak{Q} \leq 4$), indicating modest deviations from perfect regularity. In contrast, chaotic dynamics exhibit intermediate circulance values ($4 < \mathfrak{Q} < 18$), capturing the increased diversity and complexity of ordinal pattern transitions. Compar-

isons to further model systems (Appendix A), accentuate that circulance takes on similar values for higher-dimensional chaos/hyperchaos (e.g., generalized Hénon map) and stochastic time series (Fig. 3). This indicates a limitation of circulance – in its current form – due to it considering only one time series (from a specific system component or from an average over all components), assuming that this time series is representative of the system’s dynamics.

Figure 3 also demonstrates how the length of a time series N impacts on the co-domain of circulance and thus on its ability to position time series along a continuous spectrum from regularity to randomness. For shorter time series or lower embedding dimensions, the limited number of possible ordinal patterns restricts the capability of circulance to resolve dynamical regimes. As the embedding dimension decreases, circulance of chaotic time series approaches that of stochastic time series, underscoring the importance of selecting the embedding dimension such that $N \sim d!^2$ to ensure a reliable distinction between dynamical regimes.

Since the calculation of \mathfrak{Q}_τ scales approximately linear with the number of datapoints N and an accurate distinction between dynamical regimes is already possible for a few thousand datapoints, the overall approach is rather computationally efficient [54].

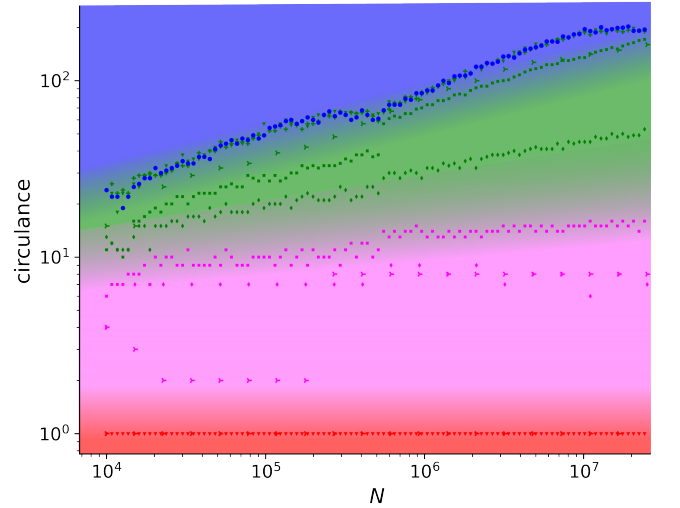


FIG. 3. Time series classification in the $\mathfrak{Q} - N$ -plane with dynamical regimes ranging from periodic via quasiperiodic and chaotic to stochastic (marker color resp. red, green, pink, and blue). Background colors schematically depict the continuum inferred empirically. Overlapping regimes between chaos and stochasticity point to limited distinguishability of high-dimensional chaos and white noise. Model systems are associated with different markers as follows: white noise - circle; generalized Hénon map - downward triangle; Zaslavskii map - plus; Hénon map - diamond; Lotka-Volterra system - square; Lorenz96 system - rotated Y. Circulance values of time series from model systems with $N = 10000$ from Table I accurately fit into the $\mathfrak{Q} - N$ -plane.

We proceed with benchmarking circulance against the largest Lyapunov exponent that is often used to distinguish between periodic and chaotic dynamics. To do so, we perform a detailed investigation of the standard Hénon map [55], which is a relatively simple dynamical system, but which, upon iteration, produces extraordinarily complex phenomena. Figure 4 illustrates the sensitivity of circulance to reflect transitions of the Hénon map as the bifurcation parameter a is varied. The alterations of circulance seen for a variation of the bifurcation parameter a resemble the ones of the largest Lyapunov exponent, and both measures distinguish between periodic and chaotic regimes. In comparison to the largest Lyapunov exponent, the range of circulance values observed for chaotic regimes identified with the largest Lyapunov exponents (Fig. 4 (c)) may allow to distinguish dynamics within these regimes in greater detail (e.g., distinguish quasiperiodicity from chaos).

B. Real World Systems

We proceed with an analysis of multi-channel electroencephalographic (EEG) data from a healthy subject. A comprehensive understanding of brain function requires careful characterization of its underlying, possibly nonlinear dynamics [57]. Investigations of EEG time series often render brain dynamics seemingly stochastic [58, 59], which may be due to the fact that the EEG only represents a one-dimensional projection of the brain's high-dimensional state-space. Yet, EEG time series have also been observed to exhibit complex behavior characterized by nonlinear dynamics [60, 61], and long-term EEG recordings are observed to also reflect influences by biological rhythms [62, 63], among others. In this context, the notion of the brain as a system that exhibits chaotic dynamics remains controversially discussed by employing methods from nonlinear time series analysis in various studies in neuroscience [64, 65]. Using a sliding-window approach (window size: 2020s, 5120 datapoints; no overlap), we computed circulance for each window – within which the system is considered approximately stationary [66] –, thereby tracking temporal fluctuations in the dynamical regime of the brain's electrical activity. These fluctuations exhibit a clear diurnal pattern (Fig. 5): circulance is elevated during daytime ($9 \leq \varphi \leq 24$), reflecting the brain's exposure to diverse sensory inputs and external perturbations during wakefulness. Circulance decreases during nighttimes ($6 \leq \varphi \leq 12$), consistent with the emergence of a more regular, rhythmic activity during sleep. Notably, we also observe the temporal evolution of circulance during nighttimes to exhibit pronounced oscillations with a period length of about 90 minutes, which potentially reflects the characteristic cycling of sleep stages [67, 68]. Ranges of circulance values may correspond to different stages within the sleep cycle, such as transitions between slow-wave (deep) sleep and rapid eye movement (REM)

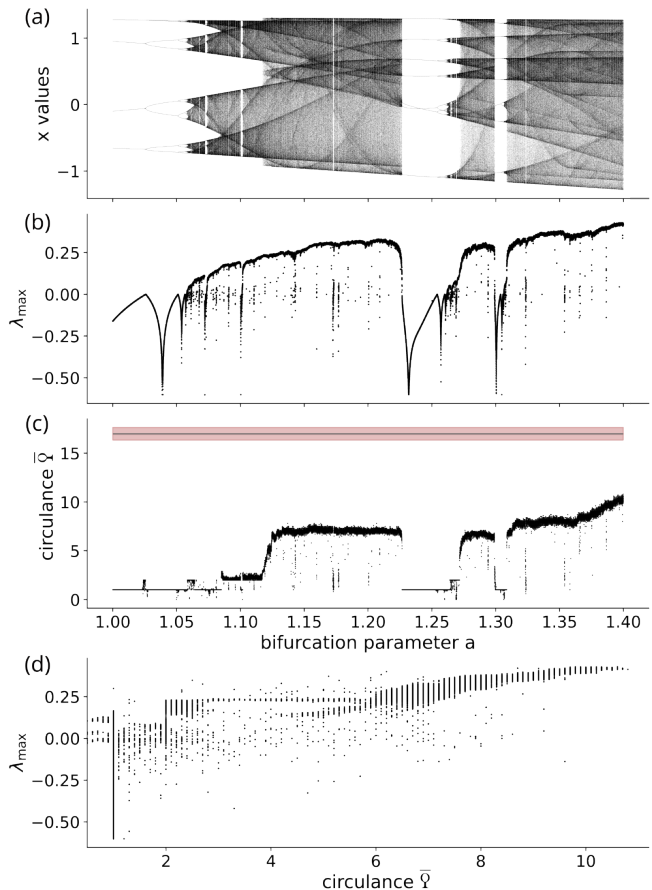


FIG. 4. Bifurcation diagram of the standard Hénon map (a). Mean largest Lyapunov exponent λ_{\max} [56] (b) and mean circulance \bar{Q} (c) of time series (x -component; $N = 10000$) for different values of the bifurcation parameter a . Each data-point is the mean of 10 realizations of time series with the same bifurcation parameter a but with different initial conditions. The gray line and the red-shaded area in (c) indicate mean and standard deviation of circulance ($\bar{Q} = 16.98 \pm 0.65$) of white noise time series of the same length and averaged over 1000 realizations. (d): Scatterplot of λ_{\max} (from (b)) and \bar{Q} (from (c)).

sleep (inset in Fig. 5). The time-dependent changes of circulance thus provide a qualitative and quantitative view into the evolving (ir)regularity of brain activity, with potential utility for distinguishing behavioral and physiological states. While the interpretation of circulance in high-dimensional, complex systems such as the brain must be approached with caution – given the limitations of single/multi-channel EEG/s as a proxy for the full system's dynamics – the observed trends are consistent with prior empirical findings. Overall, our application to EEG data suggests the potential of circulance for uncovering alterations of human brain dynamics.

Eventually, we demonstrate how circulance can possibly aid in improving understanding of solar magnetic

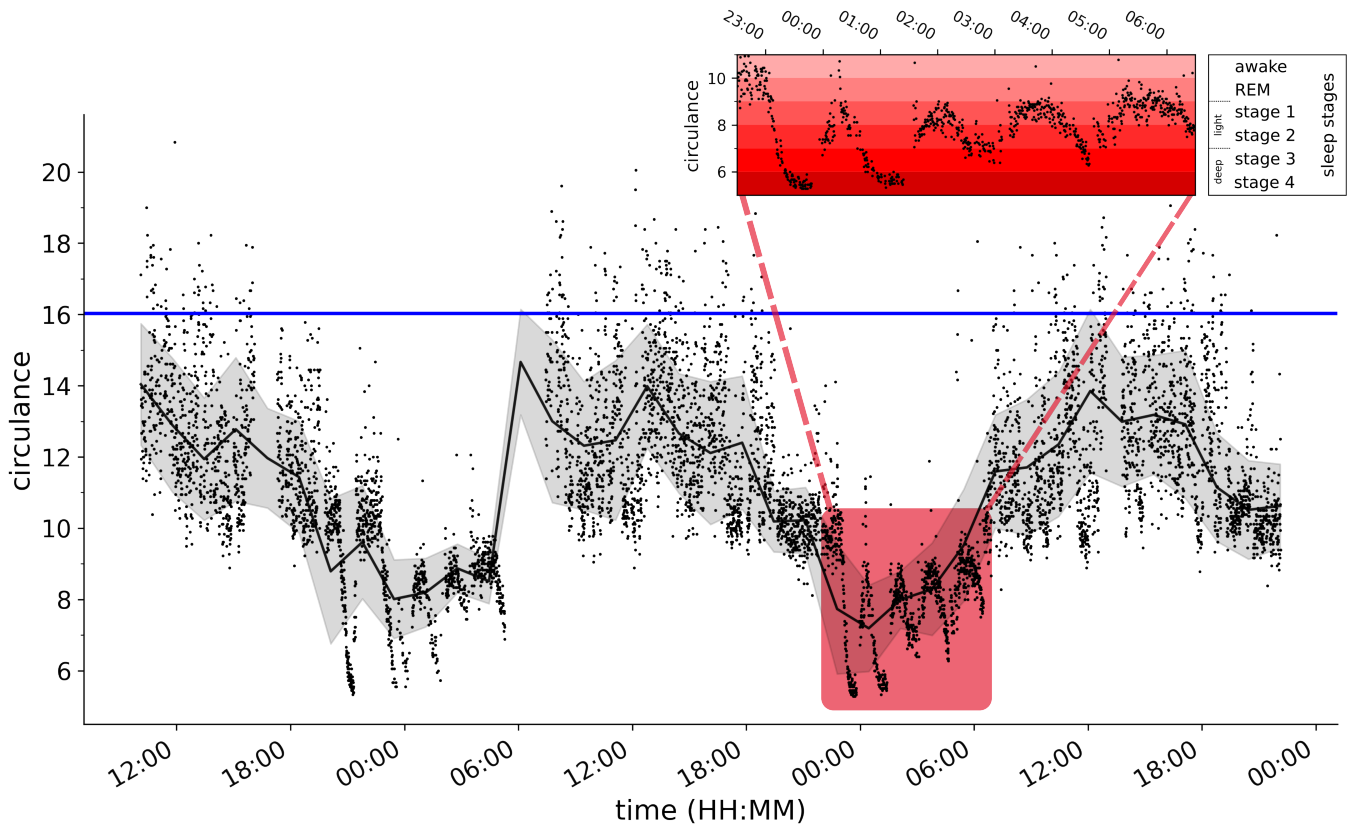


FIG. 5. Time-dependent changes of circulance (mean over all electrodes) from a multi-day EEG recording. The black line (grey shaded area) indicates the moving average (standard deviation) over 250 datapoints and serves as visual guidance. The inset schematically visualizes the potential association of ultradian rhythms during nighttimes with a sleep cycle and different sleep stages. The blue line indicates mean circulance of 100 stochastic time series with a length that equals the window size used for the sliding-window approach.

activity, which requires careful characterization of its underlying, possibly nonlinear dynamics. Investigations of sunspot number time series point to low-dimensional chaotic dynamics of the Sun's magnetic activity on shorter time scales and to seemingly stochastic dynamics on longer time scales [69, 70]. This may be due to the fact that sunspot observations only represent a low-dimensional projection of the complex high-dimensional magnetic field processes [71]. When calculated on yearly time periods employing a sliding-window approach (window size: 1 year, 365 datapoints; no overlap), circulance reveals systematic variations that do not necessarily correlate with solar cycle phases. Circulance takes values between $\varphi = 3$ and $\varphi = 7$, with a median value of $\varphi_{\text{med}} = 5$, which is smaller than the circulance value of a stochastic time series (white noise) of equal length ($\varphi = 6$). This may indicate that inter-annual fluctuations resemble properties of deterministic chaos. Notably, we observe the temporal evolution of circulance during individual ~ 11 -year sunspot cycles [72] to exhibit pronounced oscillations with characteristic time scales of 2-4 years, which potentially reflects the underlying deterministic dynamics of the solar magnetic activity. A

local minimum of circulance ($\varphi = 3$) can be observed in the middle (year 2001) of solar cycle 23, which started in August 1996 and ended in December 2008. This is in accordance with prior research [73], in which the cycle has been described as "magnetically simpler" than its closely preceding cycles (21 and 22) and therefore can be considered anomalous on a decadal timescale. When the entire multi-decadal sunspot record is analyzed as a continuous time series without cycle-based segmentation, circulance attains a significantly higher value ($\varphi = 39$) which is equal to the circulance value of a stochastic time series (white noise) of equivalent length. This may suggest that the long-term evolution of solar magnetic activity, when viewed across multiple cycles, resembles a stochastic process rather than deterministic chaos. The scale-dependence may provide quantitative indications for the dual nature of solar magnetic variability: exhibiting deterministic characteristics at the inter-annual level yet displaying stochastic properties over extended multi-decadal periods [74]. Temporal changes of circulance may thus provide both qualitative and quantitative insights into the evolving (ir)regularity of solar magnetic activity. While the interpretation of

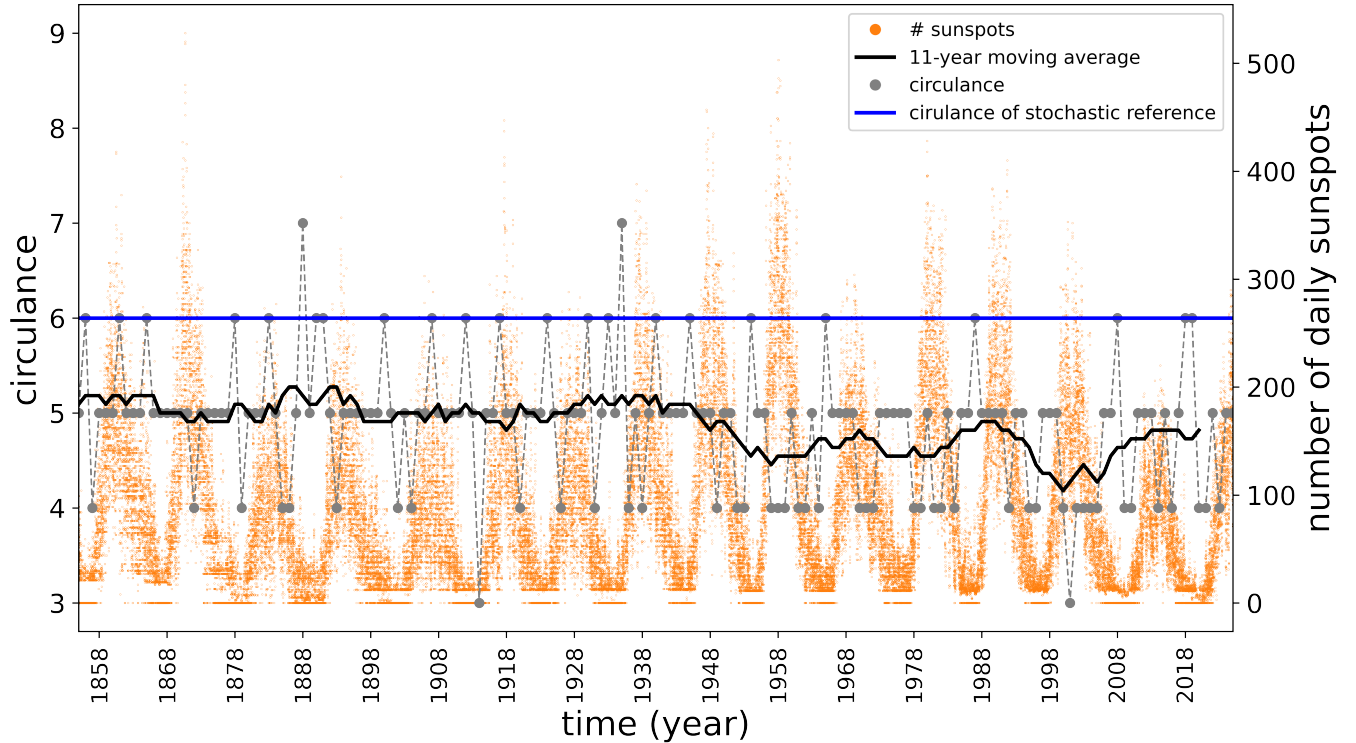


FIG. 6. Yearly changes of circulance (grey dots; dashed grey line for eye-guidance only) estimated from the daily number of sunspots (orange). The black line represents the moving average over 11 years.

circulance in high-dimensional complex systems such as the Sun must be approached with caution – and further given the limitations of sunspot number records as proxies for the solar magnetic activity [51] – the observed indicative trends are consistent with prior empirical findings from nonlinear time series analyses of sunspot numbers [69, 71, 74, 75].

Summarizing this section, the accurate characterization of predetermined dynamics of canonical model systems validates the capability of circulance for a time-series-based differentiation between periodic, quasiperiodic, chaotic and stochastic dynamics. Our application to EEG and sunspot number time series suggests the potential of circulance for tracking alterations in the dynamics of complex systems that can be associated with known states and for placing their dynamics along a spectrum from regularity to randomness.

V. CONCLUSION

We have introduced a scalar measure for classifying time series that is based on topological properties – encoding the time series’ regularity – of directed ordinal pattern transition networks (OPTNs). Circulance quantifies how much an OPTN deviates from a circular structure associated with strict periodicity. This allows a

differentiation between strictly periodic, quasiperiodic, chaotic, and stochastic regimes, while providing a quantitative metric that positions time series along a spectrum from regularity to randomness. Assuming that a time series adequately reflects the underlying system dynamics, circulance offers direct insight into the temporal organization and evolution of complex dynamical systems. Our time-series-based validation across a wide range of predetermined dynamics of canonical model systems demonstrate that circulance reliably identifies and distinguishes dynamical regimes. Our findings achieved with time-resolved analyses of circulance of real-world data hint to the possibility to facilitate the detection of transient regimes, transitions from quasiperiodicity to chaos, or more detailed classifications of dynamical states. Furthermore, integrating circulance into control strategies may support the stabilization or targeted alteration of desired dynamical states in complex systems.

Overall, circulance provides a powerful, interpretable, and computationally efficient means for positioning time series in a continuous spectrum from regularity to randomness. As a topology-based metric, it bridges nonlinear time series analysis and network theory, offering both theoretical insights and practical advantages for the study of complex systems ranging from physics to neuroscience. Beyond nuanced classification, the OPTN framework and circulance open several promising avenues for future research. We anticipate that further develop-

ments and applications of circulance, possibly even to other network representations of time series, will advance our understanding of real-world dynamical systems.

DATA AVAILABILITY

The sunspot number dataset is publicly available from Clette and Lefèvre [52]. The EEG dataset presented in this article is not readily available because it contains information that could compromise the privacy of the research participant. Requests to access this dataset should be directed to the corresponding author.

ACKNOWLEDGEMENTS

The authors would like to thank Christian Hechler and Manuel Lourenço for interesting discussions and for critical comments on earlier versions of the manuscript. This work was supported by the Deutsche Forschungsgemeinschaft and the Verein zur Foerderung der Epilepsieforschung e. V. (Bonn).

Appendix A: Details of Model Systems

If not stated otherwise, for the following systems we used the $x(x_1)$ -components as observables.

Superimposed sine waves (strictly periodic):

$$x(w) = \sin(w) + a \sin(3w) + b \sin(13w),$$

with $w \in [\alpha, \beta)$, with $\alpha = -5$ and $\beta = 5$ and parameter combinations: $(a, b) = (0, 0)$, $(1, 0)$, and $(1, 1)$ for the three cases shown in Table I. Step size is $\frac{\beta-\alpha}{N}$ according to time series length N .

Sawtooth time series (strictly periodic):

$$x(w) = w \bmod 1$$

with $w \in [\alpha, \beta)$ and $\alpha = 0$ and $\beta = 100$. Step size is $\frac{\beta-\alpha}{N}$ according to time series length N .

Van der Pol oscillator (periodic) [76]:

$$\begin{aligned} \dot{x} &= y, \\ \dot{y} &= \mu(1 - x^2)y - x, \end{aligned}$$

with damping parameters $\mu = 2$ or $\mu = 10$ for the two cases shown in Table I. Initial conditions: $(x(0), y(0)) = (0.1, 0.1)$.

FitzHugh-Nagumo oscillator (quasiperiodic) [77]:

$$\begin{aligned} \dot{x} &= x - \frac{x^3}{3} - y + I_{\text{ext}}, \\ \epsilon \dot{y} &= x + a - by, \\ I_{\text{ext}} &= I_0 + A \sin(\omega t), \end{aligned}$$

with $a = 0.7$, $b = 0.8$, $I_0 = 0$, $A = 0.9$, $\omega = 0.02$, and time scale separation parameters $\epsilon = 1/12.5$ or $\epsilon = 1/2$ for the two cases shown in Table I. Initial conditions $(x(0), y(0)) = (-1.2, -0.6)$.

Coupled FitzHugh-Nagumo oscillators (quasiperiodic/chaotic) [78]:

$$\begin{aligned} \dot{x}_i &= x_i(a - x_i)(x_i - 1) - y_i + \frac{\sigma}{O-1} \sum_{j=1}^O C_{ij}(x_j - x_i), \\ \dot{y}_i &= b_i x_i - c y_i, \end{aligned}$$

with $O = 101$ oscillators, $i \in \{1, \dots, O\}$, heterogeneous parameter $b_i = 0.006 + 0.008(i-1)/(O-1)$, and all-to-all coupling matrix $C_{ij} = 1$ for $i \neq j$, $C_{ii} = 0$. Initial conditions chosen uniformly from the interval $[0, 100]$. Coupling strengths $\sigma \in \{0.002, 0.128, 0.628\}$, $a = -0.02651$, $c = 0.02$ for the three cases shown in Table I.

Hénon map (quasiperiodic/chaotic) [55]:

$$\begin{aligned} x(n+1) &= 1 + y(n) - ax(n)^2, \\ y(n+1) &= bx(n), \end{aligned}$$

with $b = 0.3$ and bifurcation parameter $a \in \{1.1, 1.2, 1.4\}$ for the three cases shown in Table I and $n = 0, \dots, N-1$. Initial conditions: $(x(0), y(0)) = (0, 0)$.

Generalized Hénon map (periodic/chaotic) [79]:

$$\begin{pmatrix} x_1(n+1) \\ x_i(n+1) \end{pmatrix} = \begin{pmatrix} a - x_{k-1}(n)^2 - bx_k(n) \\ x_{i-1}(n) \end{pmatrix},$$

with $i \in \{2, 3, \dots, k\}$, $k = 50$, $b = 0.1$ and $a \in \{1.25, 1.75\}$ for the two cases shown in Fig. 3. $n = 0, \dots, N-1$. Initial conditions chosen uniformly from $[0, 1]$, respectively.

Lotka-Volterra model (quasiperiodic/chaotic) [80]:

$$\dot{x}_i = r_i x_i \left(1 - \sum_{j=1}^N Q_{ij} x_j \right)$$

with $i \in \{0, 1, 2, 3\}$ and

$$r = \begin{pmatrix} 1.0 \\ 0.72 \\ 1.53 \\ 1.27 \end{pmatrix} \text{ and } Q = \begin{pmatrix} 1.0 & 1.09s & 1.52s & 0.0 \\ 0.0 & 1.0 & 0.44s & 1.36s \\ 2.33s & 0.0 & 1.0 & 0.47s \\ 1.21s & 0.51s & 0.35s & 1.0 \end{pmatrix},$$

with $s = 0.97$ or $s = 1.0$ respectively for the two cases shown in Fig. 3. Initial conditions chosen uniformly from $[0.3, 0.7]$, respectively.

Zaslavskii map (chaotic) [81]:

$$\begin{aligned} x(n+1) &= (x(n) + \nu(1 + \mu y(n)) \\ &\quad + \epsilon \nu \mu \cos(2\pi x(n))) \bmod 1 \\ y(n+1) &= e^{-r}(y(n) + \epsilon \cos(2\pi x(n))) \end{aligned}$$

with $\nu = 0.095$, $\mu = 20$, $\epsilon = 0.4$ and $r = 1$ and $n = 0, \dots, N - 1$. Initial conditions: $(x(0), y(0)) = (0, 0)$.

Lorenz oscillator (quasiperiodic) [82]:

$$\begin{aligned}\dot{x} &= \sigma(y - x) \\ \dot{y} &= x(\rho - z) - y \\ \dot{z} &= xy - \beta z\end{aligned}$$

with $\sigma = 10$, $\beta = 8/3$, and control parameter $\rho \in \{155, 80\}$ for the two cases shown in Table I. Initial conditions: $(x(0), y(0), z(0)) = (1, 1, 1)$.

Lorenz 96 model (periodic/quasiperiodic/chaotic) [83]:

$$\dot{x}_i = (x_{i+1} - x_{i-2})x_{i-1} - x_i + F,$$

with $i \in \{1, 2, 3, 4, 5\}$ and periodic boundary conditions:

$$x_{i-5} = x_i = x_{i+5}$$

where $F \in \{3, 5, 8\}$ is a constant forcing term (commonly $F = 3$ for periodic, $F = 5$ for quasiperiodic and $F = 8$ for chaotic behavior; cf. Fig. 3). Initial conditions are at equilibrium ($x_i(0) = 1$).

White noise (stochastic): Gaussian white noise $x(t) \sim \mathcal{N}(0, 1)$ generated using NumPy's `numpy.random.normal` function.

Appendix B: Pseudocode

The derivation of OPTNs from time series and the computation of circulance is openly accessible as Python code on GitHub [84]. In the following, we additionally provide pseudocode for easy and quick comprehension.

1. Derivation of Ordinal Patterns

Algorithm 1 Derive Ordinal Patterns from Time Series

Require: Time series $TS \in \mathbb{R}^n$, embedding dimension $d \in \mathbb{N}$, embedding delay $\tau \in \mathbb{N}$

Ensure: Set of ordinal patterns \mathcal{P}

```

1: procedure ORDINAL_PATTERNS( $TS$ )
2:    $TS \leftarrow \text{round}(TS, 7)$   $\triangleright$  Round to 7 decimal places
3:    $n \leftarrow |TS|$ 
4:    $\mathcal{P} \leftarrow \emptyset$ 
5:   for  $i = 0$  to  $n - (d - 1)\tau - 1$  do
6:      $w \leftarrow (TS_i, ts_{i+\tau}, TS_{i+2\tau}, \dots, TS_{i+(d-1)\tau})$   $\triangleright$ 
       Extract window
7:      $\pi \leftarrow \text{argsort}(w)$   $\triangleright$  Get permutation indices
8:      $\mathcal{P} \leftarrow \mathcal{P} \cup \{\pi\}$ 
9:   end for
10:  return  $\mathcal{P}$ 
11: end procedure
```

2. Determine Embedding Dimension

Algorithm 2 Determine Embedding Dimension

Require: Time series length $N \in \mathbb{N}$

Ensure: Embedding dimension $d \in \mathbb{N}$

```

1: procedure GIVE_D( $N$ )
2:    $n \leftarrow 1, i \leftarrow 1$ 
3:   while  $n < \sqrt{N}$  do
4:      $i \leftarrow i + 1$ 
5:      $n \leftarrow n \times i$ 
6:   end while
7:   return  $i$ 
8: end procedure
```

3. Determine Maximum Embedding Delay

Algorithm 3 Determine Maximum Embedding Delay

Require: Time series $TS \in \mathbb{R}^n$

Ensure: Maximum embedding delay $\tau_{\max} \in \mathbb{N}$

```

1: procedure FIND_MAXTAU( $TS$ )
2:    $n \leftarrow |TS|$ 
3:    $\tau \leftarrow 2$ 
4:    $d \leftarrow \text{give\_d}(n)$ 
5:   while  $(d - 1)\tau < 0.1n$  do  $\triangleright$  Ensure at most 10% loss
     of data
6:      $\tau \leftarrow \tau + 1$ 
7:   end while
8:   return  $\tau - 1$ 
9: end procedure
```

4. Construction of Ordinal Pattern Transition Networks

Algorithm 4 Create Adjacency Matrix of OPTN from Ordinal Patterns

Require: Time series $TS \in \mathbb{R}^n$, embedding dimension $d \in \mathbb{N}$, embedding delay $\tau \in \mathbb{N}$
Ensure: adjacency matrix $A \in \{0, 1\}^{d \times d}$

```

1: procedure OPTN( $TS$ )
2:    $S \leftarrow \text{ordinal\_patterns}(TS, d, \tau)$     ▷ Extract ordinal
   patterns
3:    $\mathcal{U}, \mathcal{I} \leftarrow \text{unique\_with\_indices}(S)$     ▷ Get unique
   patterns and indices
4:    $m \leftarrow |\mathcal{U}|$ 
5:   Initialize adjacency matrix  $A$  with zeros
6:   for  $j = 0$  to  $|\mathcal{I}| - 2$  do
7:      $i_{\text{from}} \leftarrow \mathcal{I}[j]$ 
8:      $i_{\text{to}} \leftarrow \mathcal{I}[j + 1]$ 
9:     if  $i_{\text{from}} \neq i_{\text{to}}$  then
10:       $A[i_{\text{from}}, i_{\text{to}}] \leftarrow 1$  ▷ replace 0 with 1 if transition
      occurs
11:     end if
12:   end for
13:   return  $A$ 
14: end procedure

```

5. Main Circulance Algorithm

Algorithm 5 Computation of Circulance

Require: Time series $TS \in \mathbb{R}^n$, embedding dimension m (optional), possible embedding delays Δ (optional)
Ensure: Circulance value $c \in \mathbb{N}$, critical delay $\tau_c \in \mathbb{N}$, embedding dimension $d \in \mathbb{N}$

```

1: procedure CIRCULANCE( $x$ )
2:    $d \leftarrow \text{give\_d}(|TS|)$ 
3:    $\Delta \leftarrow \{2, 3, \dots, \text{find\_maxtau}(TS)\}$ 
4:    $Q \leftarrow \emptyset$     ▷ Initialize circulance values list
5:   for each  $\tau \in \Delta$  do
6:      $A \leftarrow \text{OPTN}(TS, d, \tau)$     ▷ Get adjacency matrix
7:      $\text{outdeg} \leftarrow \sum_{j=1}^{|A|} A_{i,j}$  for all  $i$     ▷ Calculate
     out-degrees
8:      $\text{indeg} \leftarrow \sum_{i=1}^{|A|} A_{i,j}$  for all  $j$  ▷ Calculate in-degrees
9:      $q \leftarrow |\{\text{outdeg}\} \cap \{\text{indeg}\}|$  ▷ Intersection of degree
     sets
10:     $Q \leftarrow Q \cup \{q\}$ 
11:   end for
12:    $i^* \leftarrow \arg \min_i Q[i]$     ▷ Find index of minimum
   circulance
13:    $c \leftarrow Q[i^*]$     ▷ Minimum circulance value
14:    $\tau_c \leftarrow \Delta[i^*]$     ▷ Critical embedding delay
15:   return  $c, \tau_c, d$ 
16: end procedure

```

-
- [1] H. Kantz and T. Schreiber, *Nonlinear Time Series Analysis*, 2nd ed. (Cambridge University Press, Cambridge, UK, 2003).
 - [2] J. Sun, Y. Zhao, T. Nakamura, and M. Small, From phase space to frequency domain: A time-frequency analysis for chaotic time series, *Phys. Rev. E* **76**, 016220 (2007).
 - [3] L. Lacasa, B. Luque, F. Ballesteros, J. Luque, and J. C. Nuno, From time series to complex networks: The visibility graph, *Proc. Natl. Acad. Sci. U.S.A.* **105**, 4972 (2008).
 - [4] L. Lacasa and R. Toral, Description of stochastic and chaotic series using visibility graphs, *Phys. Rev. E* **82**, 036120 (2010).
 - [5] P. Bloomfield, *Fourier analysis of time series: an introduction* (John Wiley & Sons, New York, 2004).
 - [6] G. A. Gottwald and I. Melbourne, A new test for chaos in deterministic systems, *Proc. R. Soc. A: Math. Phys. Eng. Sci.* **460**, 603 (2004).
 - [7] N. Marwan, M. C. Romano, M. Thiel, and J. Kurths, Recurrence plots for the analysis of complex systems, *Phys. Rep.* **438**, 237 (2007).
 - [8] U. S. Freitas, C. Letellier, and L. A. Aguirre, Failure in distinguishing colored noise from chaos using the “noise titration” technique, *Phys. Rev. E* **79**, 035201 (2009).
 - [9] C. W. Kulp and S. Smith, Characterization of noisy symbolic time series, *Phys. Rev. E* **83**, 026201 (2011).
 - [10] C. Kulp and L. Zunino, Discriminating chaotic and stochastic dynamics through the permutation spectrum test, *Chaos: An Interdisciplinary Journal of Nonlinear Science* **24**, 033116 (2014).
 - [11] D. M. Mateos, L. E. Riveaud, and P. W. Lamberti, Detecting dynamical changes in time series by using the Jensen Shannon divergence, *Chaos: An Interdisciplinary Journal of Nonlinear Science* **27**, 083118 (2017).
 - [12] Y. Zou, R. V. Donner, N. Marwan, J. F. Donges, and J. Kurths, Complex network approaches to nonlinear time series analysis, *Phys. Rep.* **787**, 1 (2019).
 - [13] M. R. R. Tabar, *Analysis and Data-Based Reconstruction of Complex Nonlinear Dynamical Systems: Using the Methods of Stochastic Processes* (Springer, Cham-Switzerland, 2019).
 - [14] J. R. Tempelman and F. A. Khasawneh, A look into chaos detection through topological data analysis, *Phys. D: Nonlinear Phenomena* **406**, 132446 (2020).
 - [15] J. D. Hamilton, *Time series analysis* (Princeton University Press, Princeton, NJ, 2020).
 - [16] I. Kottlarz and U. Parlitz, Ordinal pattern-based complexity analysis of high-dimensional chaotic time series, *Chaos: An Interdisciplinary Journal of Nonlinear Science* **33**, 053105 (2023).
 - [17] A. K. Angelidis, K. Goulas, C. Bratsas, G. C. Makris, M. P. Haniias, S. G. Stavriniades, and I. E. Antoniou, Distinction of chaos from randomness is not possible from the degree distribution of the visibility and phase space reconstruction graphs, *Entropy* **26**, 341 (2024).
 - [18] M. Small, D. Yu, and R. G. Harrison, Surrogate test for pseudoperiodic time series data, *Phys. Rev. Lett.* **87**, 188101 (2001).
 - [19] X. Luo, T. Nakamura, and M. Small, Surrogate test to distinguish between chaotic and pseudoperiodic time series, *Phys. Rev. E* **71**, 026230 (2005).
 - [20] Y. Zou, D. Pazó, M. Romano, M. Thiel, and J. Kurths, Distinguishing quasiperiodic dynamics from chaos in short-time series, *Phys. Rev. E* **76**, 016210 (2007).
 - [21] O. A. Rosso, H. Larrondo, M. T. Martin, A. Plastino, and M. A. Fuentes, Distinguishing noise from chaos, *Phys. Rev. Lett.* **99**, 154102 (2007).
 - [22] Z. Gao and N. Jin, Complex network from time series based on phase space reconstruction, *Chaos* **19**, 033137 (2009).
 - [23] B. Luque, L. Lacasa, F. Ballesteros, and J. Luque, Horizontal visibility graphs: Exact results for random time series, *Phys. Rev. E* **80**, 046103 (2009).
 - [24] N. Marwan, J. F. Donges, Y. Zou, R. V. Donner, and J. Kurths, Complex network approach for recurrence analysis of time series, *Phys. Lett. A* **373**, 4246 (2009).
 - [25] Y. Zou, R. V. Donner, J. F. Donges, N. Marwan, and J. Kurths, Identifying complex periodic windows in continuous-time dynamical systems using recurrence-based methods, *Chaos* **20**, 043130 (2010).
 - [26] E. J. Ngamga, D. V. Senthilkumar, A. Prasad, P. Parmananda, N. Marwan, and J. Kurths, Distinguishing dynamics using recurrence-time statistics, *Phys. Rev. E* **85**, 026217 (2012).
 - [27] S. Das, C. B. Dock, Y. Saiki, M. Salgado-Flores, E. Sander, J. Wu, and J. A. Yorke, Measuring quasiperiodicity, *Europhys. Lett.* **114**, 40005 (2016).
 - [28] F. Olivares, M. Zanin, L. Zunino, and D. G. Pérez, Contrasting chaotic with stochastic dynamics via ordinal transition networks, *Chaos: An Interdisciplinary Journal of Nonlinear Science* **30**, 063101 (2020).
 - [29] Z. Zhang, M. Zhang, Y. Chen, Z. Xiang, J. Xu, and X. Zhou, Distinguishing chaotic from stochastic dynamics via the complexity of ordinal patterns, *AIP Advances* **11**, 045122 (2021).
 - [30] B. Boaretto, R. C. Budzinski, K. L. Rossi, T. L. Prado, S. R. Lopes, and C. Masoller, Discriminating chaotic and stochastic time series using permutation entropy and artificial neural networks, *Sci. Rep.* **11**, 15789 (2021).
 - [31] T. L. Prado, B. R. R. Boaretto, G. Corso, G. Z. dos Santos Lima, J. Kurths, and S. R. Lopes, A direct method to detect deterministic and stochastic properties of data, *New J. Physics* **24**, 033027 (2022).
 - [32] W. Ren and Z. Jin, Phase space visibility graph, *Chaos Solit. Fractals* **176**, 114170 (2023).
 - [33] J. S. A. E. Fouda, W. Koepf, N. Marwan, J. Kurths, and T. Penzel, Complexity from ordinal pattern positioned slopes (copps), *Chaos Solit. Fractals* **181**, 114708 (2024).
 - [34] A. Mohan, G. Ambika, and C. Meena, Deep learning for classifying dynamical states from time series via recurrence plots, *arXiv preprint arXiv:2506.17498* (2025).
 - [35] M. B. Priestley, *Nonlinear and Non-Stationary Time Series Analysis* (Academic Press, London, 1988).
 - [36] R. Manuca and R. Savit, Stationarity and nonstationarity in time series analysis, *Phys. D: Nonlinear Phenom.* **99**, 134 (1996).
 - [37] K. Fokianos and B. Kedem, Prediction and classification of non-stationary categorical time series, *J. Multivar. Anal.* **67**, 277 (1998).
 - [38] R. Hegger, H. Kantz, L. Matassini, and T. Schreiber, Coping with non-stationarity by overembedding, *Phys. Rev. Lett.* **84**, 4092 (2000).

- [39] C. Rieke, K. Sternickel, R. G. Andrzejak, C. E. Elger, P. David, and K. Lehnertz, Measuring nonstationarity by analyzing the loss of recurrence in dynamical systems, *Phys. Rev. Lett.* **88**, 244102 (2002).
- [40] P. Fryzlewicz and H. Ombao, Consistent classification of nonstationary time series using stochastic wavelet representations, *J. Am. Stat. Assoc.* **104**, 299 (2009).
- [41] K. Lepage and D. Thomson, Spectral analysis of cyclostationary time-series: a robust method, *Geophys. J. Int.* **179**, 1199 (2009).
- [42] C. Bandt and B. Pompe, Permutation entropy - a complexity measure for time series, *Phys. Rev. Lett.* **88**, 174102 (2002).
- [43] A. M. Unakafov and K. Keller, Conditional entropy of ordinal patterns, *Phys. D: Nonlinear Phenomena* **269**, 94 (2014).
- [44] J. Zhang, J. Zhou, M. Tang, H. Guo, M. Small, and Y. Zou, Constructing ordinal partition transition networks from multivariate time series, *Sci. Rep.* **7**, 7795 (2017).
- [45] D. Cuesta-Frau, A. Molina-Picó, B. Vargas, and P. González, Permutation entropy: Enhancing discriminating power by using relative frequencies vector of ordinal patterns instead of their Shannon entropy, *Entropy* **21**, 1013 (2019).
- [46] M. Zanin and F. Olivares, Ordinal patterns-based methodologies for distinguishing chaos from noise in discrete time series, *Commun. Phys.* **4**, 190 (2021).
- [47] M. Small, Complex networks from time series: Capturing dynamics, in *2013 IEEE International Symposium on Circuits and Systems (ISCAS)* (2013) pp. 2509–2512.
- [48] M. McCullough, M. Small, T. Stemler, and H. H.-C. Iu, Time lagged ordinal partition networks for capturing dynamics of continuous dynamical systems, *Chaos: An Interdisciplinary Journal of Nonlinear Science* **25**, 053101 (2015).
- [49] A. A. Pessa and H. V. Ribeiro, Characterizing stochastic time series with ordinal networks, *Phys. Rev. E* **100**, 042304 (2019).
- [50] M. Seeck, L. Koessler, T. Bast, F. Leijten, C. Michel, C. Baumgartner, B. He, and S. Beniczky, The standardized EEG electrode array of the IFCN, *Clin. Neurophysiol.* **128**, 2070 (2017).
- [51] F. Clette, L. Svalgaard, J. M. Vaquero, and E. W. Cliver, Revisiting the sunspot number: A 400-year perspective on the solar cycle, *Space Sci. Rev.* **186**, 35 (2014).
- [52] F. Clette and L. Lefèvre, Silso sunspot number v2.0, <https://doi.org/10.24414/qnza-ac80> (2015), published by WDC SILSO - Royal Observatory of Belgium (ROB).
- [53] In some distinct and rare cases within periodic regimes of the Hénon map, the respective cirulance value can be zero.
- [54] Estimating cirulance for a time series of 10^4 data points can be performed in few milliseconds on a PC with a CPU clock rate of 3.7 GHz.
- [55] M. Hénon, A two-dimensional mapping with a strange attractor, *Commun. Math. Phys.* **50**, 376 (1976).
- [56] U. Parlitz, Identification of true and spurious Lyapunov exponents from time series, *Int. J. Bifurc. Chaos* **2**, 155 (1992).
- [57] R. G. Andrzejak, G. Widman, K. Lehnertz, P. David, and C. E. Elger, The epileptic process as nonlinear deterministic dynamics in a stochastic environment: An evaluation on mesial temporal lobe epilepsy, *Epilepsy Res.* **44**, 129 (2001).
- [58] J. P. Pijn, J. van Neerven, A. Noest, and F. H. Lopes da Silva, Chaos or noise in EEG signals: dependence of state and brain site, *Electroenceph. clin. Neurophysiol.* **79**, 371 (1991).
- [59] D. Prichard and J. Theiler, Generating surrogate data for time series with several simultaneously measured variables, *Phys. Rev. Lett.* **73**, 951 (1994).
- [60] C. J. Stam, Nonlinear dynamical analysis of EEG and MEG: Review of an emerging field, *Clin. Neurophysiol.* **116**, 2266 (2005).
- [61] S. Tong and N. V. Thankor, *Quantitative EEG analysis methods and clinical applications* (Artech House, Norwood, 2009).
- [62] K. Lehnertz, T. Rings, and T. Bröhl, Time in brain: How biological rhythms impact on EEG signals and on EEG-derived brain networks, *Front. Netw. Physiol.* **1**, 755016 (2021).
- [63] T. Bröhl, R. Von Wrede, and K. Lehnertz, Impact of biological rhythms on the importance hierarchy of constituents in time-dependent functional brain networks, *Front. Netw. Physiol.* **3**, 1237004 (2023).
- [64] K. Lehnertz, J. Arnhold, P. Grassberger, and C. E. Elger, *Chaos in Brain?* (World Scientific, Singapore, 2000).
- [65] H. Korn and P. Faure, Is there chaos in the brain? II. Experimental evidence and related models, *C. R. Biol.* **326**, 787 (2003).
- [66] K. Lehnertz, C. Geier, T. Rings, and K. Stahn, Capturing time-varying brain dynamics, *EPJ Nonlin. Biomed. Phys.* **5**, 2 (2017).
- [67] D. Aeschbach and A. A. Borbely, All-night dynamics of the human sleep EEG, *J. Sleep Res.* **2**, 70 (1993).
- [68] M. A. Carskadon and W. C. Dement, Chapter 2 - normal human sleep: An overview, in *Principles and Practice of Sleep Medicine (Fifth Edition)*, edited by M. H. Kryger, T. Roth, and W. C. Dement (W.B. Saunders, Philadelphia, 2011) 5th ed., pp. 16–26.
- [69] S. Zhou, Y. Feng, W.-Y. Wu, Y. Li, and J. Liu, Low-dimensional chaos and fractal properties of long-term sunspot activity, *Res. Astron. Astrophys.* **14**, 104 (2014).
- [70] L. Deng, B. Li, Y. Xiang, and G. Dun, Comparison of chaotic and fractal properties of polar faculae with sunspot activity, *Astron. J.* **151**, 2 (2015).
- [71] C. Letellier, L. Aguirre, J. Maquet, and R. Gilmore, Evidence for low dimensional chaos in sunspot cycles, *Astron. Astrophys.* **449**, 379 (2006).
- [72] D. H. Hathaway, The solar cycle, *Living Rev. Sol. Phys.* **12**, 4 (2015).
- [73] G. de Toma, O. R. White, G. A. Chapman, S. R. Walton, D. G. Preminger, and A. M. Cookson, Solar cycle 23: an anomalous cycle?, *Astrophys. J.* **609**, 1140 (2004).
- [74] S. Vashishtha and K. R. Sreenivasan, Bistability in the sunspot cycle, *Europhys. Lett.* **148**, 23001 (2024).
- [75] N. Jevtić, J. Schweitzer, and C. Cellucci, Research note: Nonlinear time series analysis of northern and southern solar hemisphere daily sunspot numbers in search of short-term chaotic behavior, *Astron. Astrophys.* **379**, 611 (2001).
- [76] B. Van der Pol, A theory of the amplitude of free and forced triode vibrations, *Radio review* **1**, 701 (1920).
- [77] R. FitzHugh, Impulses and physiological states in theoretical models of nerve membrane, *Biophys. J.* **1**, 445 (1961).
- [78] G. Ansmann, R. Karnatak, K. Lehnertz, and U. Feudel,

- Extreme events in excitable systems and mechanisms of their generation, *Phys. Rev. E* **88**, 052911 (2013).
- [79] G. Baier and M. Klein, Maximum hyperchaos in generalized Hénon maps, *Phys. Lett. A* **151**, 281 (1990).
 - [80] J. Vano, J. Wildenberg, M. Anderson, J. Noel, and J. Sprott, Chaos in low-dimensional Lotka–Volterra models of competition, *Nonlinearity* **19**, 2391 (2006).
 - [81] G. M. Zaslavsky, The simplest case of a strange attractor, *Phys. Lett. A* **69**, 145 (1978).
 - [82] E. N. Lorenz, Deterministic non-periodic flow, *J. Atmos. Sci.* **20**, 130 (1963).
 - [83] E. N. Lorenz, Predictability: A problem partly solved, in *Proc. Seminar on predictability*, Vol. 1, edited by T. Palmer and R. Hagedorn (Cambridge University Press, 1996) pp. 1–18.
 - [84] T. Bröhl and M. Potratzki, **OPyTN**: Ordinal pattern transition networks in Python, <https://github.com/timocbro/OPyTN> (2025).